Available online at www.sciencedirect.com
SCIENCE DIRECT®
Journal of Power Sources 150 (2005) 57–66
JOURNAL OF POWER SOURCES
www.elsevier.com/locate/jpowsour

On-board production of hydrogen for fuel cells over $Cu/ZnO/Al_2O_3$ catalyst coating in a micro-channel reactor

Xinhai Yu*, Shan-Tung Tu, Zhengdong Wang, Yunshi Qi

School of Mechanical Engineering, East China University of Science and Technology, Shanghai 200237, China

Received 20 December 2004; received in revised form 22 February 2005; accepted 28 February 2005
Available online 1 April 2005

Abstract

$Cu/ZnO/Al_2O_3$ catalyst coatings have been prepared for a micro-channel reactor, which is more suitable for on-board production of hydrogen concerning steam reforming of methanol (SRM) for fuel cells compared to conventional systems. Several parameters that control the structural characteristics of the $Cu/ZnO/Al_2O_3$ catalyst coatings have been optimized in an annular micro-reactor that is similar to the micro-channel reactor in flow pattern, but is much simpler to be fabricated and can be used repeatedly. It was confirmed that catalytic activity was directly related to copper metal surface area. The catalyst COAT-14-6 (CuO 14 wt.% and ZnO 6 wt.%) that showed the highest copper area gave the best result for SRM. A micro-channel reactor was developed by diffusion bonding and wet chemical etching. The performance of the micro-channel reactor with the optimum $Cu/ZnO/Al_2O_3$ catalyst coating has also been investigated in a continuous reaction for 100 h. The result showed the micro-channel reactor could generate enough hydrogen for power output of 10 W.

Keywords: Micro-channel reactor; Hydrogen production; Fuel cell; Coating; Steam reforming of methanol; Catalysts

1. Introduction

Today, fuel cells are considered as environmental friendly and high efficiency systems for the production of electricity, and world-widely research efforts have been made to the improvement of this technology [1]. A polymer electrolyte fuel cell (PEFC) system has been considered to be suitable to a generator for vehicles and portable applications [2]. Fuel cells need hydrogen or hydrogen-rich feed gas as fuel. Hydrogen for fuel cells can be produced in mobile units by steam reforming of methanol (SRM) because of methanol's low reforming temperatures, good miscibility with water and low content of sulfur compounds [3]. The main reactions in the proposed route may be represented by the following equations:

steam reforming of methanol:

$$CH_3OH + H_2O \rightleftarrows CO_2 + 3H_2, \quad \Delta H^0_{298} = +49.4\,\text{kJ mol}^{-1} \tag{1}$$

methanol decomposition:

$$CH_3OH \rightleftarrows 2H_2 + CO, \quad \Delta H^0_{298} = +92.0\,\text{kJ mol}^{-1} \tag{2}$$

water–gas shift reaction:

$$CO + H_2O \rightleftarrows CO_2 + H_2, \quad \Delta H^0_{298} = -41.1\,\text{kJ mol}^{-1} \tag{3}$$

Present methanol reformers are usually of fixed-bed reactors that suffer from a number of inherent problems [4]. Hot and cold spots are commonly encountered in the catalyst bed that results in poor performance [5]. This type of reactor typically has poor response to transients. Similarly, they require a prolonged time to reach working temperature from cold start-up. Micro-channel reactors are much more suitable for the distributed production of hydrogen compared to conventional systems [6]. One of the main features of micro-channel reactors is the high surface-to-volume ratio, which is several orders of magnitude higher compared to traditional chemical reactors. Micro-channel reactors work under laminar flow conditions demonstrating low-pressure drop compared to randomly fixed bed. The short radial diffusion time leads to narrow residence time distribution of gases.

* Corresponding author. Tel.: +86 21 64252363; fax: +86 21 64251804.
E-mail address: yxhh@ecust.edu.cn (X. Yu).

0378-7753/$ – see front matter © 2005 Elsevier B.V. All rights reserved.
doi:10.1016/j.jpowsour.2005.02.027

This allows optimizing the contact time of reactors avoiding the formation of unwanted by-products. Moreover, the short residence time (<0.1 s) allows a quick response to dynamic changes in the inlet conditions [7,8]. For non-stationary operations of the reactor, this feature is essential.

Recently, micro-channel fuel processors have been developed by several investigators. Holladay et al. [9] developed an integrated methanol fuel reformer system with two vaporizers/pre-heaters, a reformer, catalytic combustor and heat exchanger. Kawamura et al. developed a micro-fuel processor consisting of a vaporizer and a reformer [10]. In addition, an integrated fuel processor that has a ceramic steam reformer and catalytic chemical combustor was evaluated by Tasic et al. [11].

There are numerous reports on the catalysts for SRM. Usual catalysts are copper based. The presence of zinc oxide was found to be essential for the stability of catalyst [12]. However, there are few detailed reports on the catalyst coatings on the walls of micro-channel reactors. In this paper, preparation of the active $Cu/ZnO/Al_2O_3$ catalyst coating for a micro-channel reactor has been investigated by optimizing the catalyst composition and preparation procedure. During the optimization, an annular micro-reactor was used due to its similarity of annular micro-reactors to micro-channel reactors in flow pattern, simplicity of fabrication and repeated usage. A micro-channel reactor was developed by diffusion bonding and wet chemical etching. The performance of the micro-channel reactor with the optimum $Cu/ZnO/Al_2O_3$ catalyst coating has also been investigated.

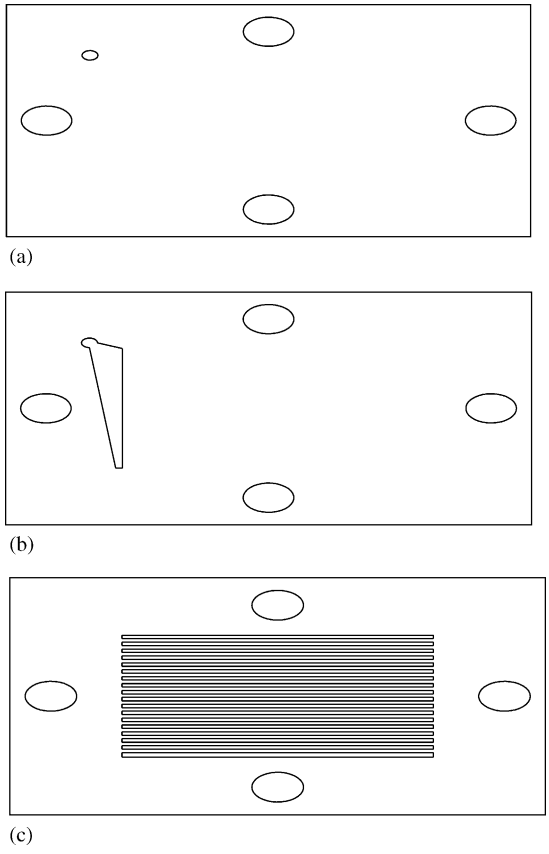

Fig. 2. Individual pattern of metal sheets: (a) cover sheet; (b) manifold sheet and (c) micro-channel sheet.

2. Experimental

2.1. Catalyst preparation

A schematic sketch of the annular micro-reactor is reported in Fig. 1. The reactor consists of an internal cylinder coaxially placed in an external tube. The gas flows downwards the annulus between the cylinder and the tube. The gap of the annulus is kept constant at 0.5 mm.

Micro-channels were patterned on the metal sheets using a wet chemical etching. Three types of patterned sheets were prepared to construct a base structure. Fig. 2 shows the individual part of a base structure. The thickness of metal sheet was 600 μm. A cover sheet has one hole, which acts as a flow path. A manifold sheet has two triangular manifolds for enhancing the uniform distribution of flow through each micro-channel. A micro-channel sheet has parallel channels of a rectangular shape on it. The micro-channel is 1000 μm wide, 600 μm deep and 32 mm long. The configuration of a base structure consists of two cover sheets, six manifold sheets and five micro-channel sheets. They were fabricated into a single structure by diffusion bonding to prepare the substrate for catalyst coating. A representative configuration of stacking is illustrated in Fig. 3. The dimensions of the micro-channel reactor were about 40 mm × 40 mm × 8 mm, respectively. Fig. 4 shows the assembled unit of the micro-channel reactor.

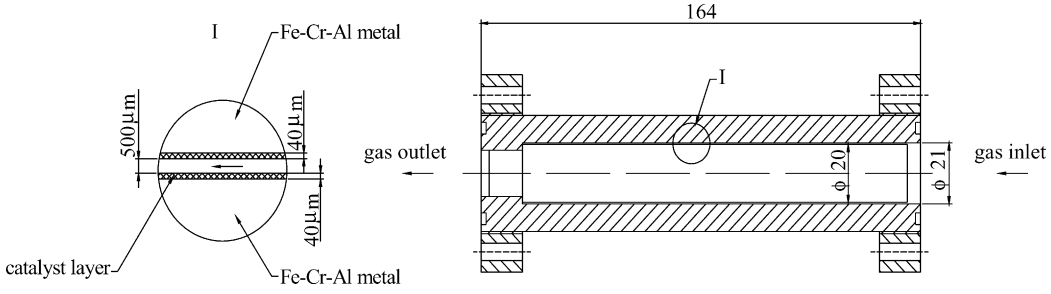

Fig. 1. Schematic diagram of the annular micro-reactor.

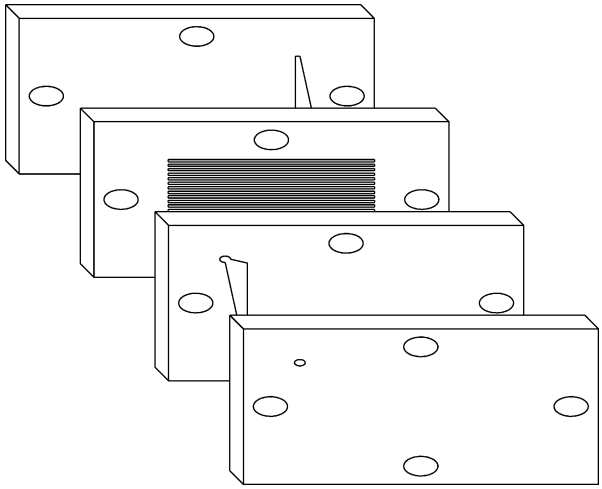

Fig. 3. Representative configuration of base structure.

The two reactors are both made of aluminium-contained stainless steel (DIN 1.4767, "Fe–Cr–Al"). By heating the alloy for approximately 5 h at 1000 °C, a thin alumina film was formed on the surface [13]. This Al_2O_3 film greatly improves the adherence of the catalyst layers on the walls of the micro-reactors. The annular micro-reactor and micro-channel reactor were initially coated with aluminium oxide (γ-Al_2O_3), to increase the surface area and to enable dispersion of the catalytic material. A γ-Al_2O_3 powder with surface area of 185 $m^2\,g^{-1}$ was ball milled for 24 h, and was subsequently added slowly into the solution of nitric acid with concentration of 2 mol l^{-1} under stirring to prepare γ-Al_2O_3 slurry. After being stirred for 30 min, the slurry was aged up to 2 h. Then, the γ-Al_2O_3 slurry was deposited on the walls of the annular micro-reactor and micro-channel reactor. After being dried in air and subsequently calcined at 500 °C, the γ-Al_2O_3 coating was formed as support for catalytically active components. Copper and zinc oxides were

Fig. 4. Photograph of the assembled reformer.

then deposited by impregnation of the γ-Al_2O_3 coating with an aqueous solution of $Cu(NO_3)_2{\cdot}3H_2O$, $Zn(NO_3)_2{\cdot}6H_2O$ (analytic grade).The catalyst coating was dried at 120 °C in air for 2 h, and subsequently, calcined at 450 °C for 4 h unless otherwise noted. The catalyst coatings thus prepared by the impregnation method are hereafter denoted as COAT-A-B, where A and B are Cu and Zn loadings in weight percent, respectively.

2.2. Catalysts characterization

2.2.1. X-ray diffraction

The crystal phase was identified by means of X-ray powder diffraction (XRD) using a Rigaku D/max 2550VB/PC. The operating parameters were monochromatic Cu Kα radiation, Ni filter, 100 mA, 40 kV, 2θ scanning from 30° to 80°, and a scan step-size 0.02°. The Cu(1 1 1) peak was employed to calculate Cu crystallite size using the Debye–Sherer equation.

2.2.2. BET surface area measurements

The specific area of the various samples was measured according to the Brunauer–Emmer–Teller (BET) theory by nitrogen adsorption using a Micrometrics ASAP 2010 instrument. Prior to adsorption measurements, the samples were degassed at least 12 h at 250 °C.

2.2.3. Scanning electron microscopy

The catalyst samples were analyzed using a JEOL JSM 6360 M scanning electron microscope (SEM) equipped with a EDAX FALCON energy dispersive X-ray spectrometry (EDS) unit.

2.2.4. Temperature programmed reduction

Temperature programmed reduction (TPR) experiments were carried out using a Micrometrics TPD/TPR 2900 instrument. Fresh calcined samples were subjected to a stream of 5% H_2 in Ar flowing at 50 $cm^3\,min^{-1}$ and increasing the temperature at 10 °C min^{-1} up to 500 °C. The current of the thermal conductivity detector was maintained at 50 mA and the detector temperature was kept constant at 100 °C.

2.2.5. Copper surface area

The surface area of copper (S_{Cu}) was determined by applying a nitrous oxide method as described by Osinga et al. [14] and Evans et al. [15] using a micromeritics TPD/TPR 2910 Autochem instrument. The catalyst samples was placed in a quartz reactor where the samples were reduced using 5% hydrogen in argon (50 $cm^3\,min^{-1}$) with a temperature ramp of 10 °C min^{-1} and dwelling at 220 °C for 2 h. The gas flow was switched to helium after the reduction and the temperature was lowered to 35 °C. Nitrous oxide was pulsed into the helium flow using a calibrated loop volume. The nitrogen formed was analyzed using the thermal conductivity detector in the TPD/TPR instrument. Unreacted nitrous oxide was separated from the gas stream using a cold trap with liquid

nitrogen as prescribed by Lemaitre et al. [16]. The content of surface copper was calculated from the nitrogen formed, assuming that dissociation of N_2O takes place on surface copper [15].

$$N_2O + 2Cu_s \rightarrow N_2 + Cu_s\text{–}O\text{–}Cu_s \quad (4)$$

The results are presented as m^2 surface copper g^{-1} catalyst assuming an even distribution of the copper surface planes. An average atomic density of 1.46×10^{19} atoms m^{-2} is assumed as proposed by Evans et al. [15].

2.2.6. XPS

X-ray photoelectron spectra (XPS) were recorded using a VG Scientific XPS with a Mg anode operating at 14 kV and 10 mA. The powder sample was supported by either double-sided carbon tape or stainless-steel disks. Charge-shift corrections were made by assuming a C 1 s signal of 285 eV. Post-reduction and post-reaction samples were sealed in He before the sample temperature was lowered to room temperature.

2.3. Catalytic activity

The set-up is shown in Fig. 5. It includes a methanol–water supply and evaporator/super-heater unit. Before entering the annular reactor, the liquid methanol–water mixture was fed from the storage tank into the evaporator by a piston membrane-metering pump (LEWA metering pump type EK-horizontal with worm gear and flange motor). The annular micro-reactor or micro-channel reactor was placed in an electrically heat furnace. The temperature of the furnace was controlled by a PID-temperature-controller with a K-type thermocouple inserted in the furnace. Two E-type thermocouples were mounted on the external wall of the annular micro-reactor or micro-channel reactor. Another two E-type thermocouples were placed at the inlet and outlet of the two reactors. The product stream composition was measured using a gas chromatograph from Varian equipped with both TCD and FID detectors. The experiments were carried out over a temperature interval of 220–300 °C. Before reaction, the catalysts were pre-reduced at 280 °C using 10% H_2 in N_2 flowing at 300 cm^3 min^{-1} for 2 h.

3. Results and discussion

3.1. Optimization of $Cu/ZnO/Al_2O_3$ catalyst coatings in an annular micro-reactor

3.1.1. Effect of ratio of Cu to Zn

As the first step of optimization, the weight ratio of Cu to Zn is varied with Cu loading from 2 wt.% to 18 wt.%. The respective preparation parameter and physical property for each catalyst are summarized in Table 1. As shown in Table 1, Cu is prone to conglomerate on the surface of the catalysts, resulting in the difference of composition between surface and bulk of the catalysts. The surface compositions ratio of Cu to Zn obtained by EDS analysis varies from 0.57 to 10.8 with bulk weight ratio of Cu to Zn from 0.11 to 9 obtained by inductively coupled plasma-atomic absorption spectrometer (ICP-AES). The variation of the weight ratio of Cu to Zn has no obvious influence on the surface areas of catalysts with the average value of 175 m^2 g^{-1}.

The TPR profiles obtained from the catalysts are illustrated in Fig. 6. Catalysts named COAT-2-18 shows two peaks. The second peak may be attributed to the stepwise reduction of copper oxide ($Cu^{2+} \rightarrow Cu^{+} \rightarrow Cu^{0}$), which perhaps indicates a strong interaction between part of the copper and zinc oxide in the sample. For the rest of the catalysts, only one distinctive peak is obtained. For the catalysts with copper loading from 2 wt.% to 18 wt.%, the lowest T_m is obtained for the catalysts with copper loading of 14 wt.%. The onset of its reduction

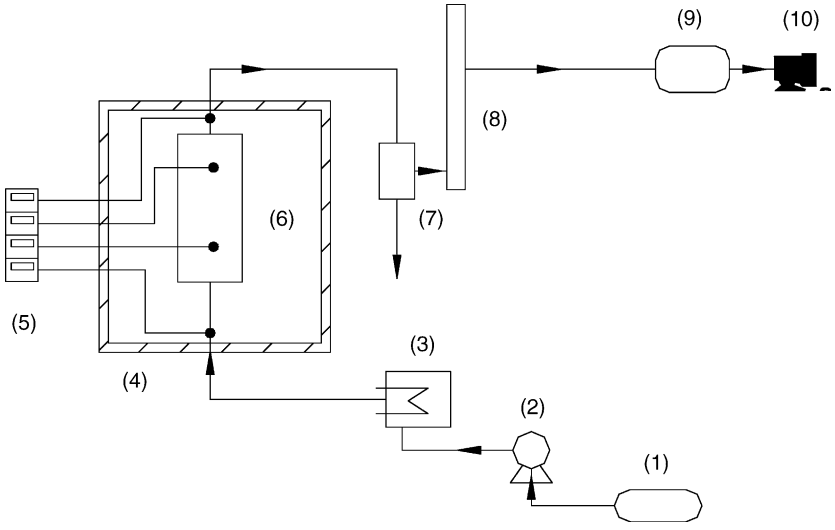

Fig. 5. Laboratory reactor system.

Table 1
Respective preparation parameters and physical properties of catalyst coatings

Catalyst name	Composition (wt.%)		Cu/Zn (wt.%) on catalysts surface	Calcinations temperature (°C)	BET ($m^2\ g^{-1}$)
	Cu	Zn			
COAT-2-18	2	18	0.57	450	176
COAT-4-16	4	16	0.76	450	173
COAT-8-12	8	12	1.43	450	178
COAT-10-10	10	10	1.73	450	174
COAT-14-6	14	6	3.58	450	175
COAT-18-2	18	2	10.8	450	174

is apparent at 170 °C. It reaches a maximum at 215 °C and completes reduction at about 270 °C.

The copper surface area is shown as a function of the copper loading in Fig. 7. The copper surface is strongly dependent on the copper loading and the maximum value is obtained with the catalyst containing 14 wt.% copper. For catalysts with higher copper content, the copper surface area is lower, probably due to the formation of large CuO crystallites resulting in loss of surface area.

The catalytic activities of the catalyst coatings with different copper loading for SRM are summarized in Table 2.

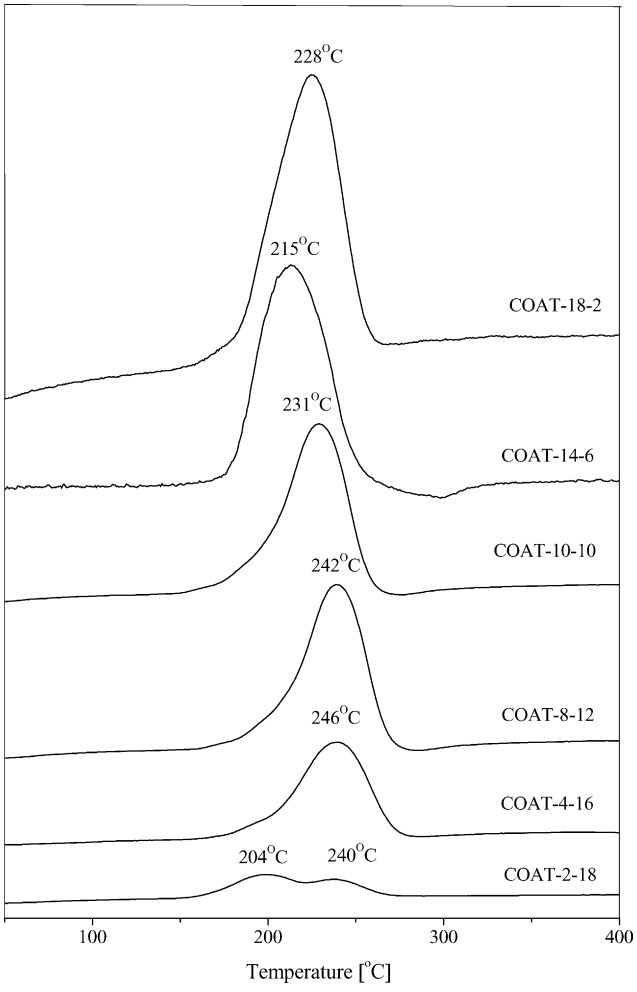

Fig. 6. TPR patterns (TCD) of the catalyst coatings.

The main products are hydrogen and carbon dioxide as well as minor product, carbon monoxide. No other products, such as dimethyl ether, methyl formate and methane, could be obtained over any of the catalyst coating tested. The methanol conversion and hydrogen production rate increase with increasing the reaction temperature. It can be seen that H_2 molar concentrations are around 70–75% and CO_2 molar concentrations are around 20–25%. The molar ratio of H_2/CO_2 is roughly around 3, indicating a typical steam reforming. COAT-2-18 with Cu loading of 2 wt.% shows the lowest activity, only around 20.6% (methanol conversion) at 242 °C. COAT-14-6 with Cu loading of 14 wt.% exhibits the highest activity to methanol conversion, around 60.4% at 242 °C. For Cu/Zn-based catalyst pellets, it is well known that their activities greatly depend on the copper surface area and the catalyst with high surface area shows better performance during SRM [17,18,19]. By correlation of copper surface areas in Fig. 7, the same correlation can also be confirmed for the $Cu/ZnO/Al_2O_3$ catalyst coatings with the COAT-14-6 of the most active catalyst coating showing the highest copper area. The activity decreases with higher copper loadings is probably attributed to the decrease in copper surface area linked to the formation of larger crystallites. In correlation with reduction properties of catalyst coating shown in Fig. 6, it is found that those with lower CuO reduction temperature show higher activity to methanol conversion during steam reform-

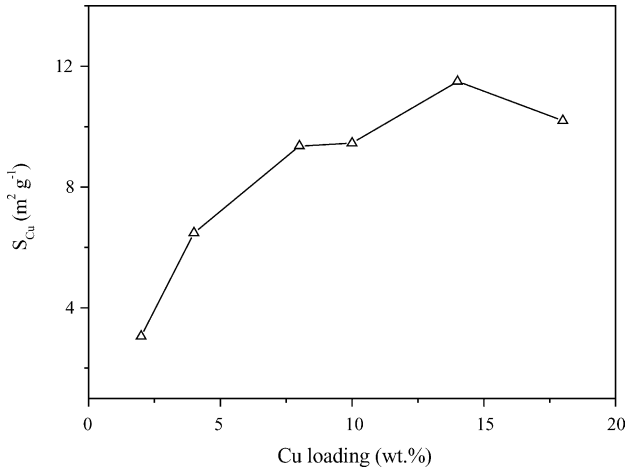

Fig. 7. Copper surface area (S_{Cu}) as a function of the copper loading of catalysts.

Table 2
Catalyst performances in steam reforming experiments

Catalysts name	Temperature (°C)	H_2 yield (mmol (s m^2)$^{-1}$)	Methanol conversion (mol%)	CO_2 selectivity (mol%)	Outlet H_2 concentration (mol%)
COAT-2-18	242	0.935	20.6	96.5	73.2
	262	2.00	44.5	94.6	72.9
	282	2.34	54.7	94.2	73.1
COAT-4-16	242	1.59	34.4	95.4	73.0
	262	2.65	58.5	94.5	73.2
	282	3.02	68.2	93.8	73.2
COAT-8-12	242	2.26	50.2	94.8	72.4
	262	3.40	76.8	93.9	72.5
	282	3.78	86.2	93.7	73.0
COAT-10-10	242	2.32	52.6	94.6	72.8
	262	3.35	76.1	94.1	72.7
	282	3.90	88.2	93.7	73.0
COAT-14-6	242	2.74	60.4	94.0	73.5
	262	3.71	81.4	93.6	74.5
	282	4.24	94.8	93.4	74.7
COAT-18-2	242	2.35	56.2	94.4	73.0
	262	3.47	78.2	94.1	73.3
	282	4.01	90.1	93.8	73.5

Reaction conditions: WHSV = 8.27 h^{-1}; (n)CH_3OH/(n)H_2O = 1/1.3.

ing. This result may be explained by the suggestion that catalyst with lower CuO reduction temperature shows better Cu dispersion and larger Cu surface [20]. Therefore, it can be concluded that the good catalytic performance is due to both highly dispersed Cu metal species and to high accessibility of the Cu species to methanol and stream.

3.1.2. Effect of metal loading

From the above results, the weight ratio of Cu/Zn is fixed at 7/3 and the total metal loading is taken as a variable from 10 wt.% to 50 wt.%. As shown in Table 3, the surface areas simply decrease with an increase in copper and zinc loading. The catalyst coating with 20 wt.% metal loading demonstrates markedly high catalytic activity at 262 °C. It can be considered that a high copper loading produces more abundant active components and leads to a decrease in surface area. Small pores originally possessed by γ-Al_2O_3 are stuffed with copper and zinc deposits as the reduction of the active surface for the catalytic reaction proceeds. This means that the optimum metal loading is 20 wt.% in the case of the coating method.

3.1.3. Effect of calcinations temperature

From the above results, the Cu and Zn loadings are fixed at 14 wt.% and 6 wt.% and the calcinations temperature is taken as a variable from 300 °C to 600 °C. As shown in Table 4, the catalyst coating after calcinations at 450 °C demonstrates the highest methanol conversion. XRD patterns of the sample after calcinations at 450 °C and 600 °C are shown in Fig. 8. The diffraction peaks of CuO are much higher in the sample after calcination at 600 °C than that at 450 °C. It indicates that calcinations at too high temperatures may result in large crystallite sizes of CuO. As it is accepted widely that CuO crystallite in a small size favors large Cu surface area after reduction, the lowest conversion of methanol over the sample after calcination at 600 °C is most probably linked to the formation of large CuO crystallite before reduction and the corresponding low copper surface area after reduction.

3.1.4. Effect of thickness of coating

The influence of the coating thickness (10 μm and 40 μm) on the catalytic activity of Cu/ZnO/Al_2O_3 coating is studied.

Table 3
Effect of metal loading on catalytic activity

Loading (wt.%)	10	20	30	40	50
Cu/Zn (wt.%)	7/3	14/6	21/9	28/12	35/15
BET (m^2 g^{-1})	182	178	141	123	119
Hydrogen yield (mmol (s m^2)$^{-1}$)	3.52	3.71	3.28	3.04	2.88
CO_2 selectivity (%)	93.9	93.6	94.1	94.3	94.4
Methanol conversion (%)	78.4	81.4	72.5	68.2	62.6

Reaction conditions: WHSV = 8.27 h^{-1}; (n)CH_3OH/(n)H_2O = 1/1.3; t = 262 °C.

Table 4
Effect of calcinations temperature on catalytic activity

Calcinations temperature (°C)	300	350	400	450	600
Cu/Zn (wt.%)	14/6	14/6	14/6	14/6	14/6
BET ($m^2\,g^{-1}$)	171	175	173	178	168
Hydrogen yield (mmol $(s\,m^2)^{-1}$)	2.58	3.30	3.43	3.71	2.30
CO_2 selectivity (%)	94.7	94.2	93.9	93.6	94.7
Methanol conversion (%)	58.3	71.8	76.2	81.4	51.2

Reaction conditions: WHSV = 8.27 h^{-1}; $(n)CH_3OH/(n)H_2O$ = 1/1.3; t = 262 °C.

The Cu, Zn loadings and calcinations temperature are fixed at 14 wt.%, 6 wt.% and 450 °C, respectively. As shown in Fig. 9, at the same space velocity, catalyst coating with smaller thickness produces the higher methanol conversion, which is consistent with most of reported results that the pellet catalyst with smaller particle produces the higher methanol conversion in a fixed-bed reactor [21]. As shown in Fig. 10, the CO level obtained from the coating of 40 μm has been found to be higher than that obtained from the coating of 10 μm at the same methanol conversion. The increase in CO concentration with increasing coating thickness can be well explained by the theory that CO is formed as a consecutive product in the reverse WGS reaction. In this theory, CO is mainly produced by the reverse WGS reaction and the concentration of CO depends on the contact time and concentrations of H_2 and CO_2. The same methanol conversion confirms the same concentrations of H_2 and CO_2 approximately. More CO is formed in the thicker coating due to its longer contact time resulting from the intra-particle diffusion limitation. As for a micro-channel reactor, the amount of active metal decreases a lot with decreasing the thickness of coating at the fixed metal loading per gram. The feed flow rate of 6 ml h^{-1} which corresponds to space velocity of 8.27 h^{-1} for the coating of 40 μm and 32.54 h^{-1} for the coating of 10 μm in the annular micro-reactor. As shown in Fig. 9, at the same feed flow rate of 6 ml h^{-1}, the methanol conversion is 94.8% over the catalyst coating of 40 μm much higher than that of 67.3% over the catalyst coating of 10 μm. As shown in Fig. 10, at the methanol conversion of 67.3%, the CO concentration is

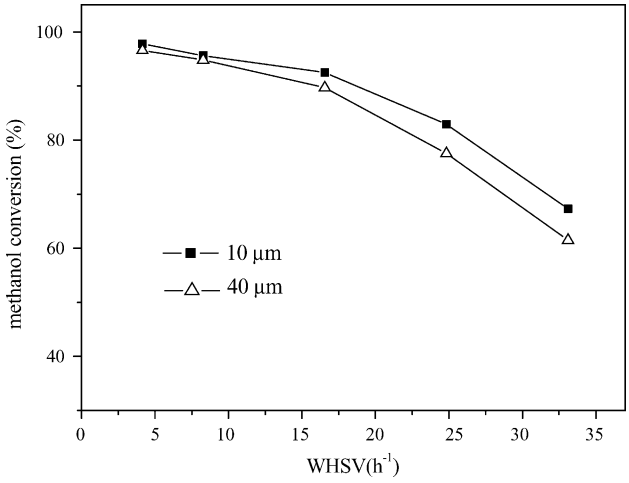

Fig. 9. Methanol conversion as a function of WHSV (h^{-1}) for COAT-14-6 with different thickness of coating (10 μm and 40 μm) (t = 282 °C, $(n)H_2O/(n)CH_3OH$ = 1.3).

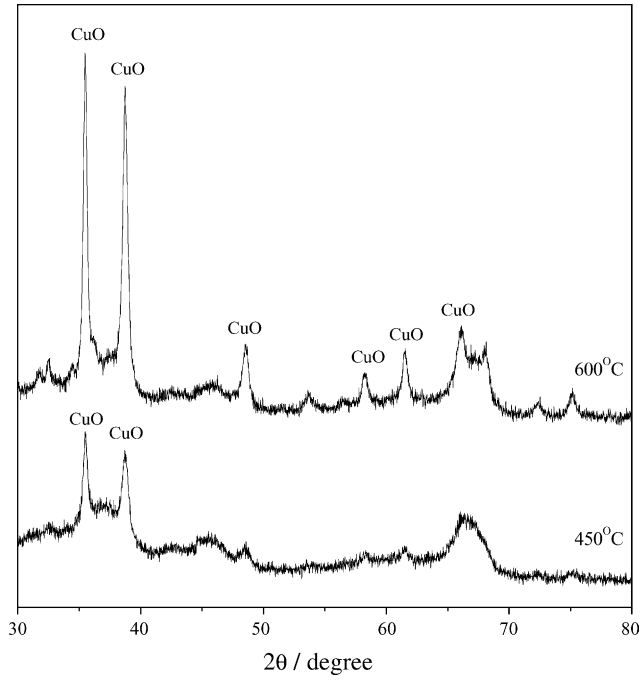

Fig. 8. XRD patterns of calcined catalysts.

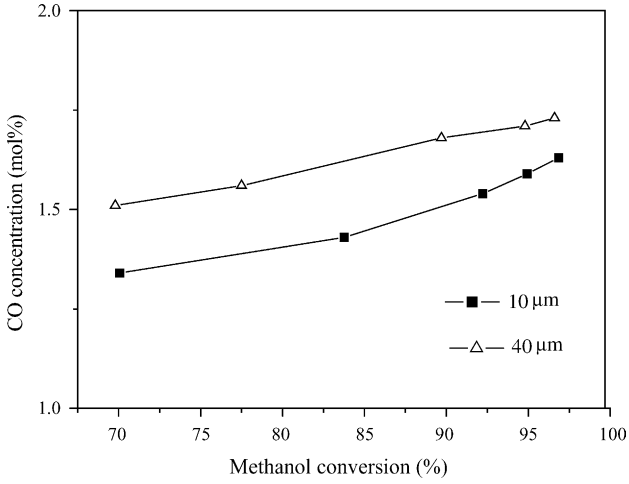

Fig. 10. CO concentration in dry reformate as a function of methanol conversion for COAT-14-6 with different thickness of coating (10 μm and 40 μm).

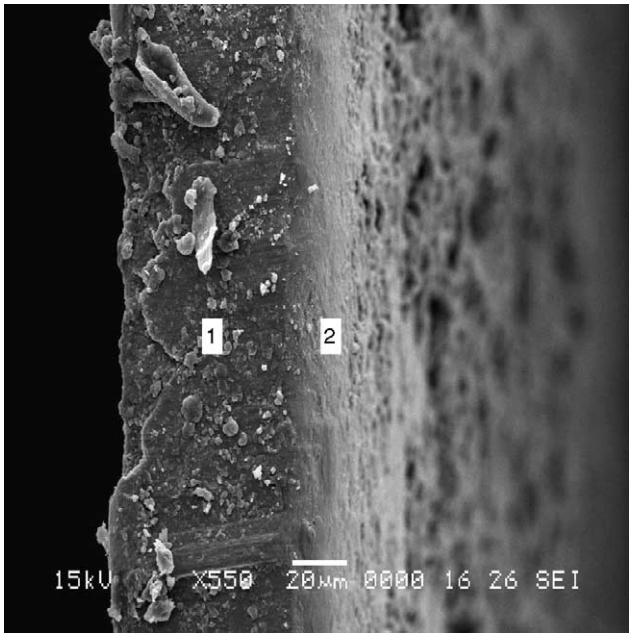

Fig. 11. SEM of γ-Al_2O_3 coating on the thermally treated metal.

1.34% over the coating of 10 μm just a little smaller than that of 1.50% over the coating of 40 μm. Therefore, the decrease of thickness of coating results in more decrease of methanol conversion than that of CO concentration at the same feed flow rate. In addition, when the thickness is over 50 μm, the adherence of coating deteriorates. Therefore, the thickness of 40 μm is better.

According to the optimization process above, COAT-14-6 is the optimum sample with parameters as follows: Cu loading of 14 wt.%, Zn loading of 6 wt.%, calcination temperature of 450 °C and thickness of 40 μm.

3.2. Characterization of COAT-14-6

Fig. 11 shows SEM images of γ-Al_2O_3 coatings on the Fe–Cr–Al alloy. The denotations of (1) and (2) stand for γ-Al_2O_3 coating and Fe–Cr–Al alloy, respectively. It shows that the adherence of γ-Al_2O_3 coating on the Fe–Cr–Al alloy is very good, without detachment or uncovered areas. A specific surface area of 183 $m^2\,g^{-1}$ was determined by the BET method. The pore size distribution of the γ-Al_2O_3 coating is shown in Fig. 12.

XRD patterns of COAT-14-6 after calcinations, reduction and reaction are shown in Fig. 13. As shown in Fig. 13(a), the diffraction peaks aluminium and zinc oxide phases are weak, which suggests that aluminium and zinc oxide phases are probably present in an amorphous-like or micro-crystallite state in the catalyst. Fig. 13(b) shows that the crystalline metallic copper phase emerges clearly after a pre-reduction using 10% H_2 in N_2 at 280 °C for 4 h. Fig. 13(c) exhibits that only Cu diffraction peaks are present in the catalyst after a continuous reaction for 100 h. The crystallite size of Cu is estimated from the half width of (1 1 1) reflection of Cu by

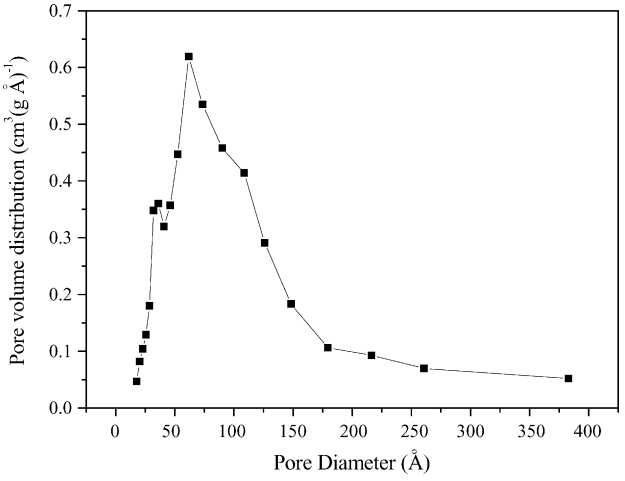

Fig. 12. Pore volume distribution of γ-Al_2O_3 coating.

Debye–Sherer equation. Compared to the D_{Cu} of 20 nm after reduction, the crystallite size of Cu increased up to 26 nm after a reaction for 100 h, which indicated sintering of Cu occurred in the reaction.

Fig. 14 shows a SEM image of the COAT-14-6. With the help of EDS analysis, it is evident that copper and zinc coexist as mixed oxide on the catalyst surface and are evenly distributed.

The COAT-14-6 was also analyzed by XPS after calcinations, reduction and 100 h reaction. As shown in Table 5, aluminium and zinc are present on the catalyst surfaces with peaks for Al 2p at 74.6–74.7 eV and Zn $2p_{3/2}$ at 1022.0–1022.2 eV. From the out-gassed fresh catalysts three components are observed at ca. 933.7 eV assigned to CuO

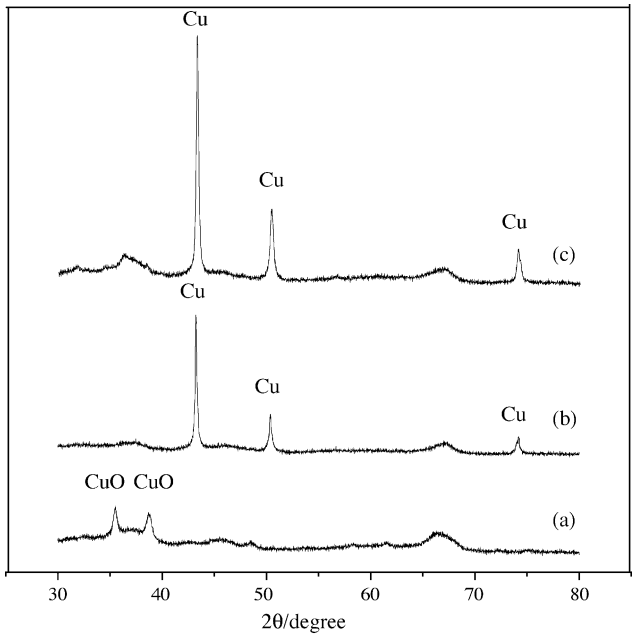

Fig. 13. XRD patterns of coated COAT-14-6: (a) before reduction by H_2/N_2, (b) after reduction by H_2/N_2 and (c) after reaction for 100 h at 282 °C.

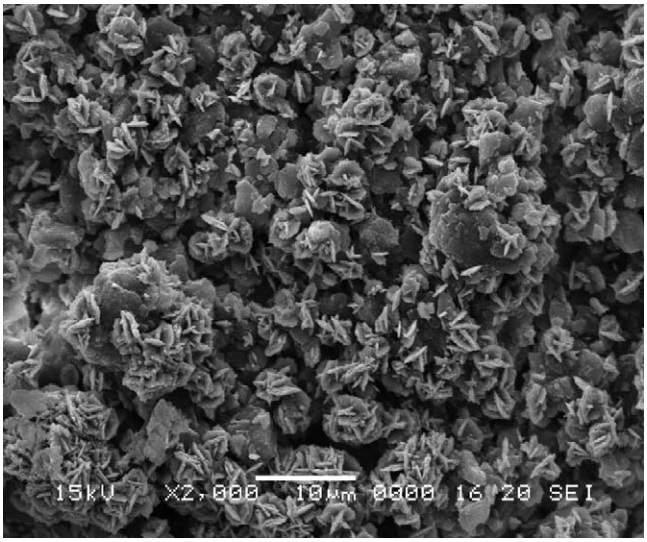

Fig. 14. SEM of COAT-14-6.

Table 5
XPS results for COAT-14-6 after being subjected to various conditions

Treatment history	Peak	BE (eV)	α_A (eV)
Calcined	Cu $2p_{3/2}$	935.4	1852.4
		934.7	1851.7
		933.7	1850.8
	Zn $2p_{3/2}$	1022.0	
	Al 2p	74.6	
Post-reaction	Cu $2p_{3/2}$	932.2	1851.4
	Zn $2p_{3/2}$	1022.1	
	Al 2p	74.7	

[22] and another Cu^{2+} species at ca. 935.4 eV and 934.7 eV which may be related either to Cu^{2+} interacting with hydroxyl groups at the ZnO surface or a $CuAl_2O_4$ spinel for the aluminium containing catalysts [23–26]. Also, a Cu^{2+} satellite peak is observed at ca. 943 eV. As shown in Fig. 15, the Cu^{2+} satellite peak disappears after reaction and the Cu $2p_{3/2}$ signal shifts down to binding energy near 932.2 eV, which may be assigned to either Cu^0 or Cu^+. As the binding energies of both Cu^0 and Cu^+ species are quite similar to differentiate which of these species are present in the catalysts, the modified Auger parameter was calculated [27–29]. Typical values of this parameter around 1851.3 eV and 1849.5 eV were found for Cu^0 and Cu^+ species, respectively. The α_A value of 1851.4 eV obtained for COAT-14-6 after reaction indicates the presence of only Cu^0 on the catalyst surface after reaction. Therefore, it can be conclude that Cu^0 is the activation center of the COAT-14-6.

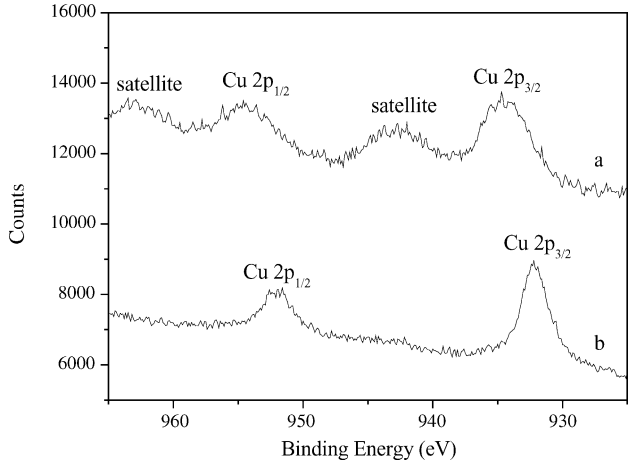

Fig. 15. Narrow scan spectra of Cu 2p for COAT-14-6: (a) after calcinations and (b) after reaction for 100 h at 282 °C.

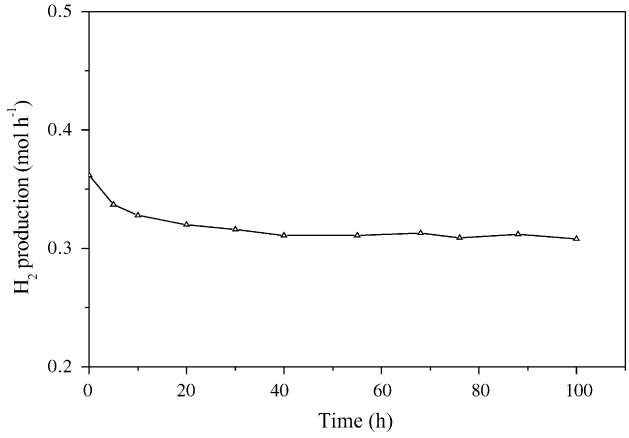

Fig. 16. Methanol conversion as a function of reaction time for COAT-14-6 in the micro-channel reactor (t = 282 °C, (n)H_2O/(n)CH_3OH = 1.3, feed flow rate of methanol and water mixture = 9 $cm^3\ h^{-1}$).

3.3. Performance of the micro-channel reactor with the COAT-14-6 on its wall

In order to investigate the catalytic activity of the COAT-14-6 on the walls of the micro-channel reactor during SRM, the continuous operation has been performed for 100 h in the condition as follows: the temperature of 282 °C, feed flow rate of 9 ml h^{-1} and the molar ratio of water to methanol of 1.3. As depicted in Fig. 16, there is an initial deactivation over the catalyst. After about 20 h, H_2 yield, methanol conversion and CO concentration are stable throughout the period at about 0.31 mol h^{-1}, 90.1% and 1.6%, respectively. Assuming 60% efficiency of fuel cell and 80% utilization of H_2, H_2 yield of 0.31 mol h^{-1} means the estimated power output is 10 W.

4. Conclusions

Preparation of the active $Cu/ZnO/Al_2O_3$ catalyst coatings for a micro-channel reactor has been investigated by optimizing the catalyst composition and preparation procedure. It was confirmed that the catalytic activities of the catalyst coatings are directly related to the copper metal surface areas. COAT-14-6 is the optimum sample with parameters as follows: Cu loading of 14 wt.%, Zn loading of 6 wt.%, calcination temperature of 450 °C and thickness of 40 μm. X-ray

photoelectron spectra and X-ray diffraction patterns indicate that Cu^0 is the activation center of COAT-14-6. The performance of the micro-channel reactor with COAT-14-6 on its wall indicates that the developed micro-channel reactor can generate enough hydrogen for power output of 10 W.

References

[1] G. Cacciola, V. Antonucci, S. Freni, J. Power Sources 100 (2001) 67.
[2] Y. Tanaka, T. Utaka, R. Kikuchi, K. Sasaki, K. Eguchi, Appl. Catal. A 238 (2003) 11.
[3] G.-G. Park, D.J. Seo, S.-H. Park, Y.-G. Yoon, C.-S. Kim, W.-L. Yoon, Chem. Eng. J. 101 (2004) 87.
[4] H.G. Düsterwald, B. Höhlein, H. Kraut, J. Meusinger, R. Peters, U. Stimming, Chem. Eng. Technol. 20 (1997) 617.
[5] J.C. Amphlett, L.M. Keams, R.F. Mann, B.A. Peppley, J.P. Salrador, R.A.J. Dams, P.R. Hayter, S.C. Moore, Proceedings of the Intersociety of Energy of Energy Conversion and Engineering Conference, vol. 34, 1999, p. 395.
[6] P. Reuse, A. Renken, K. Haas-Santo, O. Görke, K. Schubert, Chem. Eng. J. 101 (2004) 133.
[7] A. Rouge, B. Spoetzl, S. Schenk, K. Gebauer, A. Renken, Chem. Eng. Sci. 56 (2001) 1419.
[8] A. Rouge, A. Renken, Proceedings of the Fifth International Conference of Microreaction Engineering (IMRET 5), Springer, Strasbourg, 2001, p. 230.
[9] J.D. Hollady, E.O. Jones, M. Phelps, J. Hu, J. Power Sources 108 (2002) 21.
[10] Y. Kawamura, N. Ogura, T. Katsumata, A. Igarashi, Proceedings of 2002 Fuel Cell Seminar, 18–21 November, Palm Springs, CA, 2002, p. 669.
[11] S. Tasic, D. Gervasio, R. Koripella, S.P. Rogers, S. Samms, J. Hallmark, Proceedings of 2002 Fuel Cell Seminar, 18–21 November, Palm Springs, CA, 2002, p. 275.
[12] G.A. El-Shobaky, G.A. Fagal, M. Mokhtar, Appl. Catal. A 155 (1997) 167.
[13] K. Haas-Santo, M. Fichtner, K. Schubert, Appl. Catal. A 220 (2001) 79.
[14] Th.J. Osinga, B.G. Linsen, W.P. van Beek, J. Catal. 7 (1967) 227.
[15] J.W. Evans, M.S. Wainwright, A.J. Bridgewater, D.J. Young, Appl. Catal. 7 (1983) 75.
[16] J.L. Lemaitre, P.G. Menon, F. Delannay, in: F. Delannay (Ed.), Characterization of Heterogeneous Catalysts, Marcel Dekker, New York, 1984, p. 299.
[17] B. Lindström, L.J. Pettersson, P.G. Menon, Appl. Catal. A 234 (2002) 111.
[18] M.L. Cubeiro, J.L.G. Fierro, Appl. Catal. A 168 (1998) 307.
[19] L. Ma, G. Gong, T. Trans, M.S. Wainwright, Catal. Today 63 (2000) 499.
[20] S. Velu, K. Suzuki, M. Okazaki, M.P. Kapoor, J. Catal. 194 (2000) 373.
[21] H. Purnama, T. Ressler, R.E. Jentoft, H. Soerijanto, R. Schlögl, R. Schomäcker, Appl. Catal. A 259 (2004) 83.
[22] G.G. Jernigan, G.A. Somorjai, J. Catal. 147 (1994) 567.
[23] A. Sepulveda, C. Marquez, I.R. Ramos, A.G. Ruiz, J.L.G. Fierro, Surf. Interface Anal. 20 (1993) 1067.
[24] A. Wolberg, J.L. Ogilvie, J.F. Roth, J. Catal. 19 (1970) 206.
[25] B.R. Strohmeier, D.E. Leyden, R.S. Field, D.H. Hercules, J. Catal. 94 (1985) 514.
[26] G. Ertl, R. Hierl, R. Knozinger, N. Thiele, H.P. Urbach, Appl. Surf. Sci. 5 (1980) 49.
[27] C.D. Wagner, L.H. Gale, R.H. Raymond, Anal. Chem. 51 (1979) 466.
[28] Y. Okamoto, K. Fukino, T. Emanaka, T. Teranishi, J. Chem. Soc. Chem. Commun. (1982) 1405.
[29] T.H. Fleish, R.L. Mieville, J. Catal. 90 (1984) 165.